Multiple ionization of CO due to electron impact

Cechan Tian* and C. R. Vidal
Max-Planck-Institut für Extraterrestrische Physik, P.O. Box 1603, 85740 Garching, Germany
(Received 23 September 1998)

The absolute cross sections of all the possible dissociation channels following the electron-impact multiple ionization of CO have been measured. The cross sections of the channels corresponding to the production of ion pairs are measured by coincidence techniques. Those of the channels associated with neutral fragments are obtained indirectly. At high excitation energies, the total cross sections of different stages of ionization show an exponential decrease as the ionization stage increases. The cross sections of different channels reveal the internal dissociation dynamics of the dissociation following the multiple ionization of the molecules. The appearance potentials corresponding to different dissociation channels are also measured, which show that the ground states of triply and quadruply ionized CO are nearly Coulomb-like because the Coulomb interactions inside the molecules are stronger. [S1050-2947(99)10302-0]

PACS number(s): 34.80.Gs, 34.50.Gb

I. INTRODUCTION

In recent years the dynamics of the multiple ionization of molecules and the structures of the multiply charged molecules have attracted growing attention [1]. The determination of the structures and bonding arrangements of the multiply charged molecules can lead to a wealth of information about the nature of the interatomic interactions. Recently, continuous efforts have been made to gain a better, more quantitative insight into the structure of the ions themselves and into the mechanisms and kinematics involved in their reactions. Studies of the multiply charged molecules continue to present a serious theoretical as well as experimental challenge. The high density of the electronic states in such species makes accurate calculations rather difficult and demands the use of *ab initio* quantum-chemical methods well beyond the simple Hartree-Fock level. The relatively high energies required for their formation and the intrinsic instability of the ions complicate the experiments. Despite the relatively simple and stable structures of the doubly charged molecules, the knowledge of the electronic structure of most doubly charged molecules is still ambiguous. So far N_2^{2+} and NO^{2+} are the only two molecules on which rotationally resolved spectra have been achieved [1]. N_2^{2+} was studied with the photofragment spectroscopy [2–4], whereas NO^{2+} was studied with the technique of photoemission spectroscopy [5,6]. The experiments on the doubly charged molecules include the threshold photoelectron coincidence spectroscopy of a number of diatomic molecules [7,8], photoion-photoion coincidence measurement of the ionic fragments [9–13], electron impact ionization [14], and Auger electron-ion coincidence spectroscopy [15]. The theoretical work on the doubly charged molecules consists mostly of the calculation of the lowest electronic states [10,16,17]; some of these levels have been observed experimentally [2,3,10]. In the case of triple and higher ionization, the existing experimental results are mostly from intense excitation such as heavy-ion collisions [18,19] and high-intensity laser ionization [20,21] except for a few results obtained with photoion-photoion coincidence [11] and electron-impact experiments [22]. The theoretical work on the multiple ionization of molecules is mostly from Handke *et al.* [23–25] who calculated the electronic states of the triply ionized CO.

In this paper we report the absolute cross sections of the ion-pair formation channels of carbon monoxide due to electron impact for electron energies from threshold to 600 eV. From the cross sections of the ion-pair formation of CO and our previous results on the electron-impact ionization of CO [26], the absolute cross sections of the possible dissociation channels of CO at different ionization stages are derived.

The cross section of electron-impact ionization is proportional to the square of the transition matrix element for the transition from the initial to the final state, to the density of the final states, and to the inverse of the incident velocity [27]. The absolute ionization cross sections will provide the density of the state distribution of the multiply ionized molecules. In their theoretical work Handke *et al.* [23–25] calculated the electronic states of the triply ionized carbon monoxide. They derived the relative cross sections for the triple ionization of CO and compared it with the relative-cross-section measurement of Spekowius and Brehm [22]. We hope that the present absolute cross sections of triple ionization will provide some further information on the triple ionization of CO. Furthermore, the results on the double and quadruple ionization of the present work will provide an additional understanding about the structure and the dissocation dynamics of multiply ionized molecules.

II. EXPERIMENT

A. Experimental setup

In order to measure the cross sections of ion-pair formation produced by the dissociation of the multiply ionized CO, the two ions must be measured by coincidence techniques. The experimental setup consists of a crossed molecular and an electron beam and a focusing time-of-flight mass spectrometer that are similar to those in previous work and have been described in detail [28,26,29]. Briefly, a continuous

*Present address: Department of Physics, Texas A&M University, College Station, TX 77843-4242.

molecular beam is crossed with a pulsed electron beam (100 ns) at right angles. The molecular beam is produced by a gas flow from a long needle with an inner diameter of 0.4 mm passing through a skimmer. The top of the needle is about 2 cm above the skimmer and the skimmer is about 6 cm above the electron beam. The interaction region is less than $4\times4\times4$ mm^3. About 100 ns after the decay of the electron beam a pulsed voltage is applied to the extraction mesh of the mass spectrometer. The ions are extracted into a specially designed focusing time-of-flight (FTOF) mass spectrometer. The shield plates in the interaction region of the FTOF mass spectrometer cause the extraction mesh to perform as a plane-convex lens, which focuses the ions close to the axis of the FTOF mass spectrometer as the ions leave the ion source region. It also reduces the divergence angle with respect to the extraction system of a normal Wiley-McLaren time-of-flight mass spectrometer. The flight tube of the FTOF mass spectrometer is segmented into two tubes of identical length with a fine mesh in between. The fine mesh performs as a spherically symmetric lens if the voltage applied to it is about 1.3–1.4 times the voltage on the flight tubes. The detection plane is thus the image of the acceleration plane. In order to make the system more efficient in collecting the energetic ions produced by multiple ionization, the voltages on the extraction mesh, the flight tubes, and the focusing lens are increased compared to those in previous work [28,26]. In the experiments the voltage applied to the extraction mesh is typically -0.85 kV, that on the flight tubes is -1.75 kV, and that on the focusing mesh is -2.33 kV [29].

As described in detail in a previous publication [28], the focusing effect of the present time-of-flight mass spectrometer raises significantly the tolerance of the detection system with respect to the initial kinetic energy and the starting position of the ions. Ion trajectory calculations show that with the present voltage settings the ions with an initial kinetic energy as high as 25 eV per charge can be collected with the same efficiency as the thermal ions in the focusing time-of-flight mass spectrometer [29]. The kinetic-energy release of the triple ionization of CO has been measured by Spekowius and Brehm [22]. We can see that the kinetic energy of the ions is well within the collection capability of the present setup. For quadruple ionization, no data on the kinetic-energy release exist due to electron-impact ionization. The kinetic-energy release of quadruple ionization due to fast ion-beam collisions was measured by Sampoll *et al.* [18] and Mathur *et al.* [19]. If the kinetic-energy release due to the electron impact is similar to that due to a fast ion beam, we are confident that more than 90% of the ions produced by quadruple ionization are collected by the present setup.

The major difference of the present experiment with respect to the previous work is the coincidence technique. For the selective and exclusive detection of the products for multiple ionization of molecules, the ionic fragments have to be detected by coincidence. Two coincidence techniques have been developed. In the first technique the coincidence measurement is done with the conventional coincidence electronics. In the second coincidence technique we study the covariance mapping mass spectroscopy of the fragments [20,21].

B. Coincidence electronics

1. Configurations

The ion signal output from the microchannel plate is amplified by a preamplifier and sent into two gated constant fraction discriminators. The threshold of the constant fraction discriminators is set so that the ion signal can pass and the noise is eliminated. If we want to measure the ion pair, e.g., C^{2+}-O^+, the gate of the first discriminator is adjusted so that only C^{2+} can pass. Its output is sent to the multichannel scaler (MCS) as the start signal. The second discriminator is ungated so that all the ion signals can pass. Its output is sent to the MCS as the stop signal. In this way we obtain all the ions that are produced in the same electron shot together with the C^{2+} ions. The typical coincidence time-of-flight mass spectra, with C^{2+} as the start signal, are shown in Fig. 1(b). For comparison, a mass spectrum with an extraction trigger as the start signal is shown in Fig. 1(a). We call it a normal mass spectrum. The time offset has been changed so that it can be shown on the same time scale with the coincidence mass spectrum.

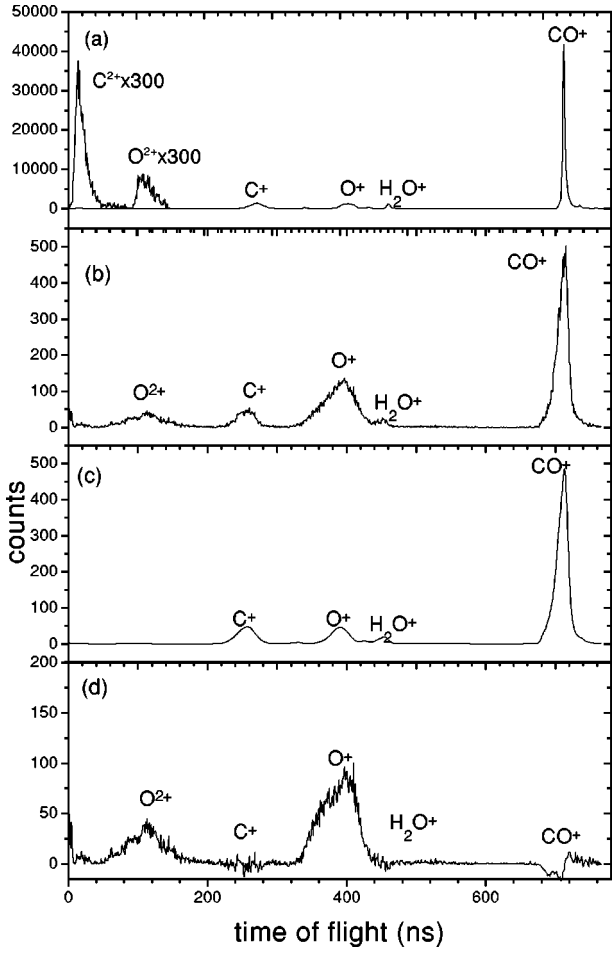

FIG. 1. (a) Normal time-of-flight mass spectrum at an electron energy of 600 eV. (b) Measured coincidence mass spectrum with C^{2+} as the start signal. (c) Calculated false coincidence mass spectrum with C^{2+} as the start signal. (d) After subtracting (c) from (b), a spectrum containing only true coincidence events is obtained.

2. Removal of false coincidence

If we check the mass spectrum in Fig. 1(b), we see that the ions that show mass peaks are O^{2+}, C^+, O^+, H_2O^+, and CO^+. However, in the dissociative ionization of a CO molecule, no process such as

$$CO^{3+}\rightarrow C^{2+}+CO^{+} \tag{1}$$

can occur. The observation of CO^+ indicates that false coincidence contributes to the observed mass spectra. The appearance of the H_2O^+ peak further demonstrates the existence of the false coincidence. In order to get accurate cross-section data, we must remove the false coincidence in the mass spectra.

In order to remove the false coincidence, we assume that the probability for the occurrence of a false ion-pair coincidence is proportional to the probability for the production of each ion of the pair. In the case of C^{2+} as the start signal, the probability of the occurrence of a false coincidence event at the time bin x can be described by

$$p(x)=\int_{C^{2+}_{\min}}^{C^{2+}_{\max}} N_{C^{2+}}(x_1)N(x_1+x)dx_1, \tag{2}$$

where $N(x_1)$ is the probability for the occurrence of an ion event at time bin x_1 in a normal time-of-flight mass spectrum. $C^{2+}_{\min}$ and $C^{2+}_{\max}$ are the minimum and maximum time bins of the mass peak of C^{2+} in the normal mass spectrum. We get the probability for the production of the ions from the normal mass spectrum when the trigger of the extraction voltage is sent to the MCS as the start signal. We use Eq. (2) to calculate the probability for the occurrence of a false coincidence event with different ions as the start signal. The scale is normalized to the mass peak of CO^+ in the corresponding measured mass spectrum.

The calculated false coincidence mass spectrum is shown in Fig. 1(c), with C^{2+} as the start signal. We subtract the false coincidence from the measured coincidence mass spectra. We thus get the mass spectrum with only true coincidence events. The achieved mass spectra are shown in Fig. 1(d). Because we scaled the calculated mass spectrum to the measured mass spectrum at the mass peak of CO^+, we see that the mass peak of CO^+ has disappeared in the final mass spectrum. However, the mass peak of C^+ has also almost vanished because in the dissociative ionization of CO the process

$$CO^{3+}\rightarrow C^{2+}+C^+ \tag{3}$$

cannot occur either. From this we conclude that the false coincidences in the mass peaks of O^{2+} and O^+ are eliminated.

Here we note that there is the possibility of overestimating the false coincidence in such a subtraction process. In measuring the cross section of the ion pair of C^++O^+, if the cross section of the ion pair is not much smaller than the cross section for the production of O^+, the calculated false coincidence mass peak of C^++O^+ may contain considerable amounts of true coincidence events. In order to avoid such an overestimate, we reduce the count rate in the measurements so that the false coincidence count rate is much lower than the total count rate. In this way we try to avoid large errors in the measurements. In measuring the cross section of the ion pair of $C^{2+}+O^+$, C^++O^{2+}, and $C^{2+}+O^{2+}$, this problem does not exist because the cross sections for these ion pairs are much smaller than those for the corresponding ions.

3. Normalization and error estimate for the cross section of the ion-pair formation

After we obtain the mass spectra only with the true coincidence, we can get the absolute cross sections for the ion-pair formation by normalizing the coincidence counts to the counts of the start events and the cross section values of the start ions. We measured the cross sections of the ions in our previous work [26]. The start signal is also counted during the measurement. In the example of $C^{2+}+O^+$, the absolute cross section values are obtained by

$$\sigma(C^{2+}+O^+)=\frac{n_{\text{coincidence}}}{n_{\text{start}}T\eta}\sigma(C^{2+}), \tag{4}$$

where n represents the counts of the coincidence and the start, respectively. T is the total transmission of the meshes in the time-of-flight mass spectrometer. η is the detection efficiency of the microchannel plate. We get the transmission of the meshes from the measurement of the optical transparency and the open area ratio from the manufacturer's manual. The two data agree with each other. We get $T=51.1\%$. For the detection efficiency of the multichannel plate, we use the open area ratio from the manufacturer's manual, which is 60%. It has been proved experimentally by a number of authors that the detection efficiency of the microchannel plate is equal to its physically open area ratio [30–32].

C. Covariance mapping mass spectroscopy of CO

In the second coincidence technique we measured the cross sections of the ion pairs by studying the covariance mapping mass spectroscopy of the ions. The technique of covariance mapping mass spectroscopy was developed by Frasinski *et al.* [20,21]. In this technique the normal trigger is used as the start signal of the MCS. In every single shot the autocorrelation function of the spectrum is calculated. After a long-time accumulation the mass spectra and the coincidence spectra are shown in a two-dimensional time-of-flight mass spectrum as in Fig. 2. The present experimental technique and the normalization procedures have been described before [29]. A spectrum containing single events is also recorded at the same time, which is used to subtract the false coincidence in a way similar to that of Bruce *et al.* [14]. The covariance mapping mass spectrum after the removal of the false coincidence is shown in Fig. 3. Comparing Fig. 2 with Fig. 3, we can clearly see that the orientation of the false coincidence islands is determined by the shapes of the corresponding mass peaks. The orientation is usually horizontal. However, the orientation of the true coincidence islands is determined by the momentum and charge associated with the corresponding ionic fragments. In Figs. 2 and 3 the orientation of C^++O^+ is close to 45°. However, the orientation of $C^{2+}+O^+$ and C^++O^{2+} islands is at a steeper angle since doubly charged fragments are involved. Since the electric field in the interaction region is inhomogeneous, we do not want to compare the orientation angles with the calculations directly. The absolute cross section of ion pairs is obtained by

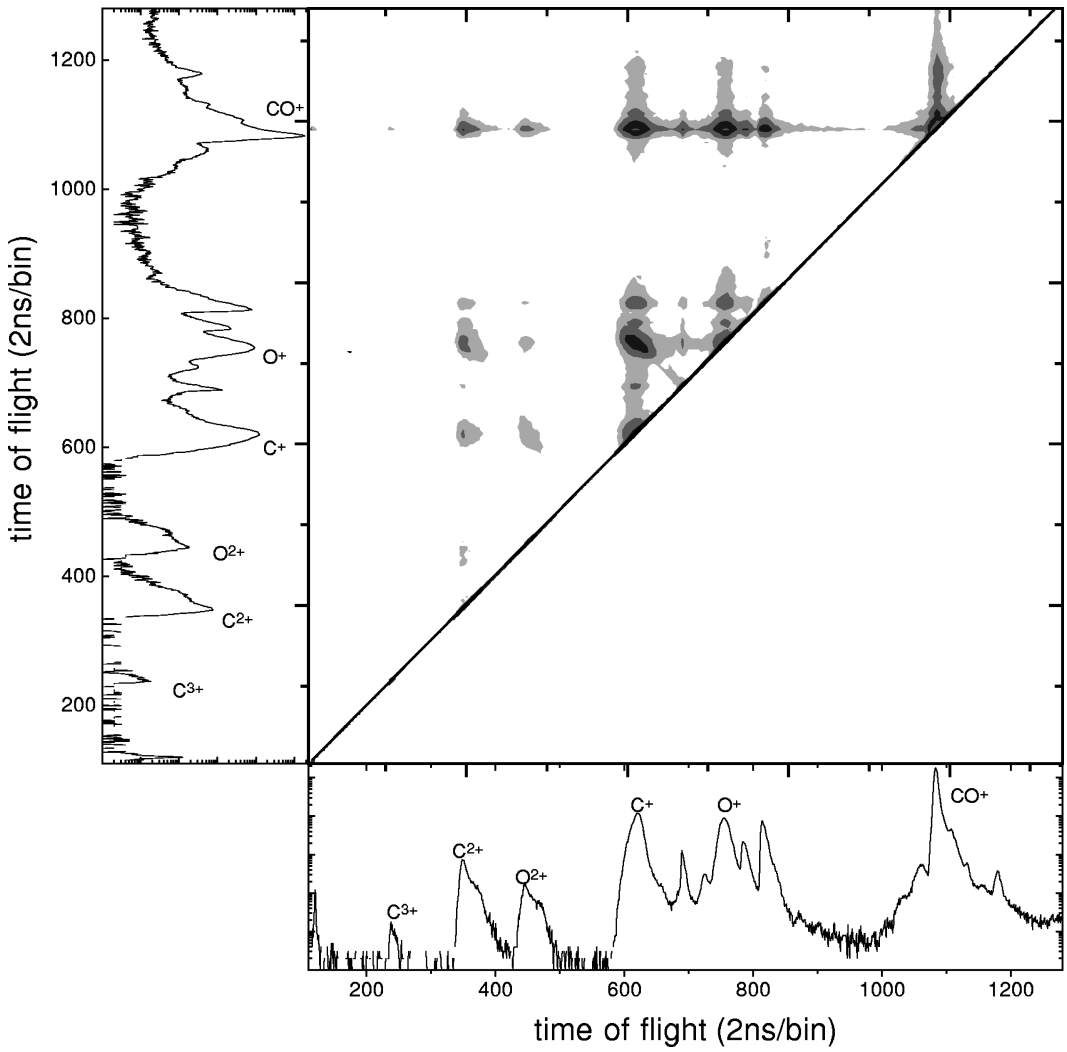

FIG. 2. Covariance mapping mass spectrum of CO at the electron energy of 200 eV.

$$\sigma(C^{2+}+O^{+})=\frac{n_{\text{coincidence}}}{n_{\text{total}}T\eta}\sigma(\text{total}), \tag{5}$$

where n_{total} is the total number of ions. σ(total) is the total ionization cross section of CO. T and η are identical to those in Eq. (4).

Compared to the first coincidence technique, the method of covariance mapping has the advantage of detecting all the ions and the ion pairs at the same time. The experiment is thus less time consuming. The relative values of the cross sections are also more accurate.

D. Error estimate

The errors in the first technique originate mainly from data fluctuations, the error of the cross-section values of the start ions ($\sim$15%), the deviation of the transparency of the meshes to the ions compared to that of light, and the subtraction of the false coincidence. The technique of covariance mapping introduces smaller errors in the relative amplitude since all the ions and ion pairs are measured at the same time [29]. We expect that the overall error of the absolute value is about 25% for the data above 1×10^{-19} cm^2. For those with smaller values, the error is higher. We estimated it to be 30 $-$40 %.

E. Derivation of the cross sections of the other channels

In the multiple ionization of CO, we did not observe the existence of stable CO^{3+} and any ions with charge in excess of 3. The different possible dissociation channels are listed in the following: single ionization,

$$CO^{+}\rightarrow CO^{+} \tag{6}$$

$$\rightarrow C^{+}+O \tag{7}$$

$$\rightarrow C+O^{+}; \tag{8}$$

double ionization,

$$CO^{2+}\rightarrow CO^{2+} \tag{9}$$

$$\rightarrow C^{+}+O^{+} \tag{10}$$

$$\rightarrow C^{2+}+O \tag{11}$$

$$\rightarrow C+O^{2+}; \tag{12}$$

triple ionization,

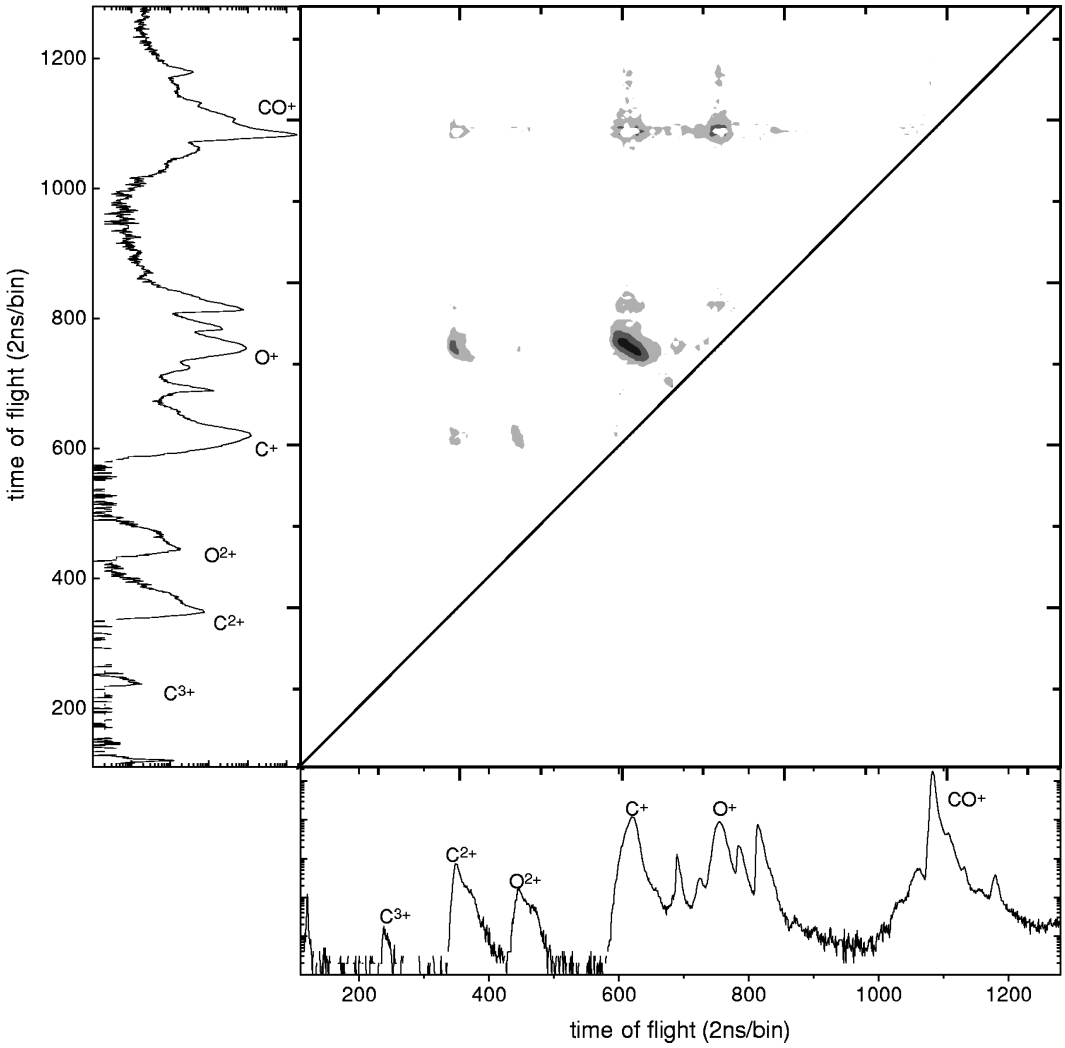

FIG. 3. Same as Fig. 2, after the false coincidence events are removed.

$$CO^{3+} \rightarrow C^{2+} + O^{+} \quad (13)$$

$$\rightarrow C^{+} + O^{2+} \quad (14)$$

$$\rightarrow C^{3+} + O \quad (15)$$

$$\rightarrow C + O^{3+}; \quad (16)$$

and quadruple ionization,

$$CO^{4+} \rightarrow C^{2+} + O^{2+} \quad (17)$$

$$\rightarrow C^{3+} + O^{+} \quad (18)$$

$$\rightarrow C^{+} + O^{3+}. \quad (19)$$

From the above equations we can clearly see which channels contribute to the production of the ionic fragments. Since we already got the absolute cross sections for these products [26], we can obtain in the present work the absolute cross sections of the ion-pair channels. Therefore, we can deduce the cross sections of the other listed channels that cannot be measured directly. Here we want to note that the polar dissociation channels such as $CO \rightarrow C^{+} + O^{-}$ and $CO \rightarrow C^{-} + O^{+}$ also contribute to the production of the positive ions. In the present work we cannot get the cross sections for these channels. However, these cross sections are expected to be negligibly small compared to those of the channels to be deduced.

III. RESULTS

A. Dissociation channels

Single ionization has three possible channels, as listed in Eqs. (6)–(8). The products of the three channels are CO^{+}, $C^{+} + O$, and $C + O^{+}$, respectively. The cross sections for these three channels are shown in Fig. 4 and are listed in Table I. The cross section of the production of CO^{+} is from our previous paper [26]. We also measured this value in our present experiment again. The results agree with the previous measurement. We see that among all the channels of single ionization, the most preferred one is the formation of stable CO^{+} because most of the lowest levels of CO^{+} are the stable and long-lived ones [33].

The four possible reaction channels after double ionization of CO are listed by Eqs. (9)–(12). The cross sections for these channels are shown in Fig. 5 and are tabulated in Table II. The data for CO^{2+} are from our previous paper [26]. In the present work these data were measured again. They agree

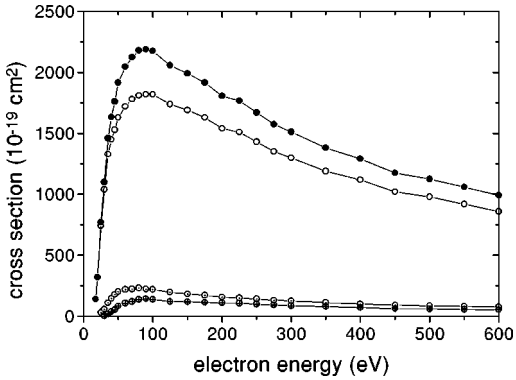

FIG. 4. Cross sections of the possible reaction channels after the single ionization of CO. The products are CO^+ (-○-), $C^+ + O$ (-⊙-), and $C + O^+$ (-⊕-). The total cross section of single ionization is shown by -●-.

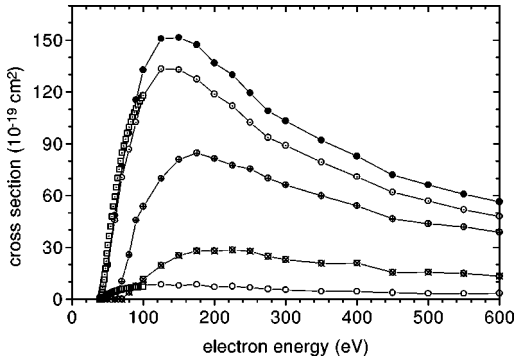

FIG. 5. Cross sections of the possible reaction channels after the double ionization of CO. The products are CO^{2+} (-○-), $C^+ + O^+$ (-⊙-), $(C^{2+} + O) \times 10$ (-⊕-), and $(C + O^{2+}) \times 10$ (-⊗-). The total cross section of double ionization is shown by -●-. The calculated data are also included, as shown by box symbols. For more details see the text.

with the previous results within the experimental errors. We see that after the double ionization of CO, the reactions are dominated by the separation of the CO^{2+} into the two ionic fragments of $C^+ + O^+$. The lowest electronic levels of CO^{2+} are characterized by a deep minimum and a high barrier against dissociation into $C^+ + O^+$. The potential wells support a number of metastable vibrational levels, located far above the dissociation limit. The lower ones are very long lived, while the levels close to the potential maximum may tunnel through the potential barrier on time scales down to picoseconds [1,7,8]. The higher electronic levels are mostly strongly repulsive levels [10]. Some branch of the excitation of the CO molecules to the lowest electronic levels results in metastable CO^{2+}, which is the origin of the measured CO^{2+}. The excitation to higher electronic levels results mainly in unstable CO^{2+}, which subsequently dissociates into $C^+ + O^+$. The ion pair of $C^+ + O^+$ appears at about 38 ± 2 eV, even before CO^{2+} (42 ± 1 eV). As pointed out by Lablanquie *et al.* [10] and Masuoka and Nakamura [11], the production of the ion pair of $C^+ + O^+$ at the low electron energies is due to the autoionization of $(C\,O^+)^*$.

Since no data exist for direct comparison with the present experiments, the only data we can refer to is the photoionization cross sections measured by Masuoka and Nakamura for the photonenergies from threshold to 100 eV [11]. In

TABLE I. Cross sections (in unit of 10^{-19} cm^2) of different channels of single ionization of CO.

Energy (eV)	$C^+ + O$	$C + O^+$
25	31.0	
30	57.0	3.00
35	110	20.0
40	146	38.0
45	179	53.2
50	201	84.4
60	220	107
70	224	120
80	233	138
90	224	144
100	218	138
125	197	121
150	183	118
175	172	113
200	157	109
225	151	107
250	142	98.9
275	131	93.0
300	127	84.9
350	112	78.9
400	101	70.7
450	92.9	62.8
500	86.0	59.9
550	81.4	56.4
600	78.3	53.4

TABLE II. Cross sections (in unit of 10^{-19} cm^2) of different channels of double ionization of CO.

Energy (eV)	CO^{2+}	$C^+ + O^+$	$C^{2+} + O$	$C + O^{2+}$	Total
45	0.01	10.7			10.8
50	0.84	19.5			20.4
60	2.63	45.7			48.5
70	5.34	70.6	1.09		77.0
80	6.22	86.8	2.79	0.40	95.9
90	7.57	102	4.57	0.76	115
100	8.21	118	5.36	1.15	132
125	8.60	133	6.99	1.95	150
150	7.88	132	8.09	2.53	151
175	8.51	127	8.47	2.79	147
200	6.97	118	8.14	2.78	136
225	7.45	111	7.76	2.85	129
250	6.69	102	7.56	2.77	119
275	5.85	93.6	7.01	2.47	109
300	5.48	88.9	6.62	2.28	103
350	4.57	79.4	5.98	2.08	92.0
400	4.50	70.8	5.41	2.09	82.8
450	3.72	62.0	4.66	1.54	71.9
500	3.31	56.9	4.37	1.57	66.2
550	3.29	51.8	4.19	1.48	60.7
600	3.35	47.8	3.87	1.32	56.4

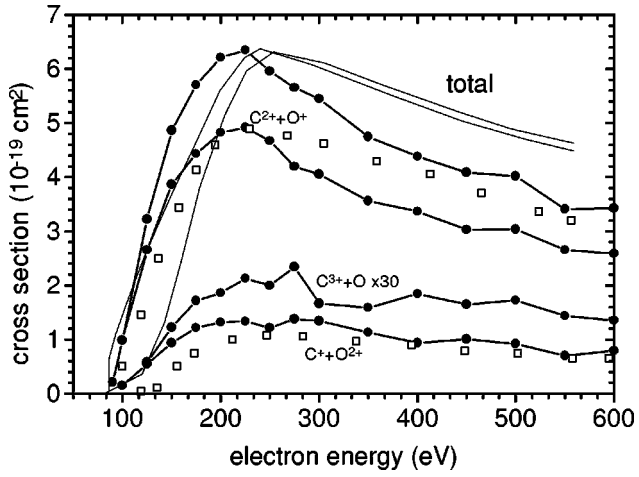

FIG. 6. Cross sections of the channels $C^{2+}+O^{+}$, $C^{+}+O^{2+}$, and $(C^{3+}+O)\times 30$ after the triple ionization of CO. -●-, present work; □, Spekowius and Brehm [22]; ——, Handke *et al.* [23].

photoionization the cross section is proportional to the oscillator strength of the transition at the photon energy. However, in electron-impact excitation the electrons excite all the possible transitions within the excitation energy range. The cross section is approximately proportional to the integral of the oscillator strengths of all the possible transitions. In this crude picture, we calculated the electron-impact ionization cross sections of the ion pair $C^{+}+O^{+}$ and CO^{2+} from the photoionization cross section of Masuoka and Nakamura and normalized the calculated value of $C^{+}+O^{+}$ to the experimental result at 100 eV. The results are also shown in Fig. 5. We see that the relative cross section of $(C^{+}+O^{+})/CO^{2+}$ shows excellent agreement with the experimental results. Although in the measurement of Masuoka and Nakamura the time window of detection of CO^{2+} is slightly different from the present work, we hope to show that the amplitude of the present results on ion-pair formation are in reasonable agreement with the photoionization cross section of Masuoka and Nakamura [11].

The main pathways of the dissociation after the triple ionization of CO are the channels of ion-pair formation, which are described by Eqs. (13) and (14). The cross sections for these two channels are shown in Fig. 6 and are isted in Table III. Those of the channels associated with the neutral products are expected to be small. Handke *et al.* [23–25] calculated the electronic states of the triply ionized CO. They suggested that there might be some electronic states with very shallow potential wells. However, no stable CO^{3+} was observed in the experiment.

The cross sections for the two ion-pair formation channels of the triple ionization were also measured by Spekowius and Brehm [22]. Since no absolute values were given in their work, we normalized their results on $C^{2+}+O^{+}$ to our absolute value at 250 eV. We see that the two measurements then show reasonable agreement with respect to the relative values of the two channels. The agreement on the relative shape of the two measurements on the channel of $C^{2+}+O^{+}$ is not satisfactory. We believe that the present measurements are more accurate since the experimental arrangement of Spekowius and Brehm discriminated strongly against fast ions. At different electron energies, the kinetic-energy distributions of the ions are possibly different. The discrimination against fast ions may result in a variable collection efficiency and the subsequent inaccurate measurement of the relative shapes. Handke *et al.* [23–25] calculated the total cross section of the triple ionization. The result is also included in Fig. 6. No absolute data were given in their work. We normalized their results to our total cross section value at 250 eV. We see that their calculation then shows good agreement with the present measurements.

TABLE III. Cross sections (in unit of 10^{-19} cm^2) of different channels of triple ionization of CO.

Energy (eV)	$C^{2+}+O^{+}$	$C^{+}+O^{2+}$	$C^{3+}+O$	Triple total
90	0.21			0.21
100	0.99	0.15		0.99
125	2.65	0.54	0.019	3.22
150	3.87	0.94	0.041	4.87
175	4.43	1.21	0.057	5.70
200	4.82	1.32	0.062	6.21
225	4.91	1.34	0.071	6.34
250	4.67	1.22	0.067	5.96
275	4.20	1.37	0.078	5.65
300	4.05	1.34	0.056	5.45
350	3.56	1.13	0.053	4.74
400	3.37	0.93	0.062	4.38
450	3.02	1.00	0.055	4.09
500	3.03	0.92	0.057	4.01
550	2.65	0.70	0.048	3.41
600	2.58	0.79	0.045	3.43

In the work of Spekowius and Brehm, the authors obtained a very crude absolute-cross-section value for the triple ionization at 1000 eV. For the channels (13) and (14) they measured the relative cross section of triple ionization with respect to the total ionization cross sections and got the values of 6.7×10^{-4} and 1.3×10^{-4} for $\sigma^{3+}/\sigma^{\text{total}}$ at 1000 eV, which corresponds to about 7×10^{-20} and 1.4×10^{-20} cm^2, respectively. If we extrapolate the absolute values to 600 eV along their curves, the absolute values for these two channels at 600 eV will be around 1.0×10^{-19} and 0.2×10^{-19} cm^2. Those values are smaller than the present results by a factor of 5. If the absolute values of Spekowius and Brehm were accurate and we normalized our measurements on ion-pair formation to their value, all the absolute cross sections of ion-pair formation in the present work would have to be decreased by a factor of 5. This would change the relative value of $C^{+}+O^{+}+$ to CO^{2+} significantly. The agreement between the present work and that of Masuoka and Nakamura [11] on the relative production of $C^{+}+O^{+}$ and CO^{2+} confirms that the present measurements on the absolute cross sections of triple ionization are accurate.

The cross sections for the reaction channels $C^{2+}+O^{2+}$ and $C^{3+}+O^{+}$ after quadruple ionization are shown in Fig. 7 and are listed in Table IV. The error is about $30-40\,\%$ because of the extremely small values. The cross sections for the other channels after the quadruple ionization are smaller than 2×10^{-21} cm^2 at an electron energy of 600 eV. No experimental or theoretical results exist for comparison. We

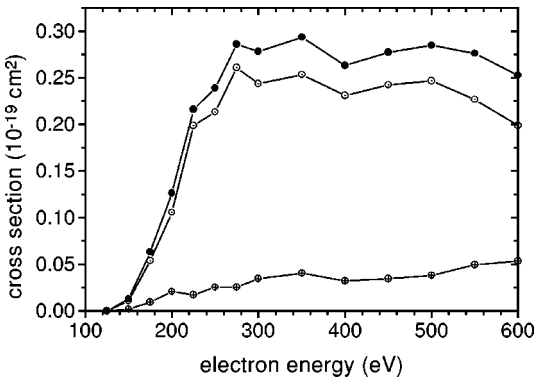

FIG. 7. Cross sections of the channels $C^{2+}+O^{2+}$ (-⊙-) and $C^{3+}+O^{+}$ (-⊕-) after quadruple ionization of CO. -●- denotes the total cross section.

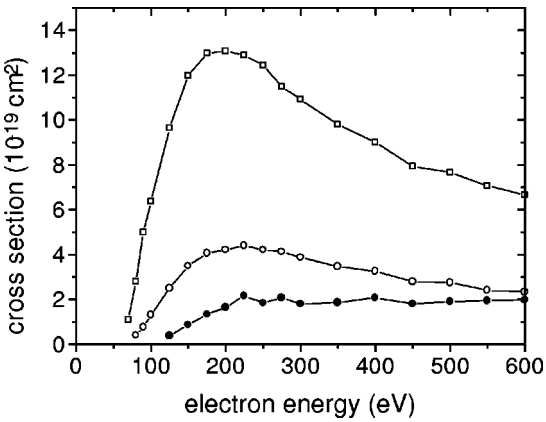

FIG. 8. Cross sections for the production of C^{2+} (-□-), O^{2+} (-○-), and $(C^{3+})\times 30$ (-●-) versus the electron energy.

see that the channel of equal charge separation dominates the dissociation.

The cross section for the production of C^{3+} was not reported before. It is shown in Fig. 8 and Table V. The data for C^{2+} and O^{2+} have been reported before by the present authors [26]. The present results agree with the previous data within the experimental errors despite the different experimental settings. They are also shown because the present data fluctuations are smaller.

B. Neutral production

The absolute cross sections associated with the production of neutral fragments are also obtained in this work after we neglected the contributions from the polar dissociation channels. As shown above, we have obtained the absolute cross sections for the channels (7), (8), (11), (12), (15), and (16), which are associated with the production of neutral fragments. The sum of Eqs. (7), (11), and (15) and that of Eqs. (8), (12), and (16) give us the absolute production of the neutral fragments O and C during the electron-impact dissociative ionization of CO, respectively. A number of authors were engaged in the measurements of the cross sections of electron-impact dissociation into neutral fragments [34,35]. However, in such work the normalization of the cross section to absolute values is usually difficult. In the present work the absolute cross sections for the dissociative ionization into the neutral fragments are obtained indirectly. For the total production of neutral O and C, the contribution from the dissociation of neutral CO must be considered. Cosby measured the absolute production of neutral C and O from electron impact dissociation of CO [36]. The total of his results and the present result will give us the absolute production of C and O from electron-impact excitation of CO.

TABLE IV. Cross sections (in unit of 10^{-19} cm^2) of different channels of quadruple ionization of CO. The last coloumn is the cross section for C^{3+} production.

Energy (eV)	$C^{2+}+O^{2+}$	$C^{3+}+O^{+}$	Total	C^{3+}
125				0.019
150	0.011	0.002	0.013	0.063
175	0.054	0.01	0.063	0.067
200	0.10	0.021	0.12	0.083
225	0.19	0.017	0.21	0.10
250	0.21	0.025	0.23	0.092
275	0.26	0.025	0.28	0.10
300	0.24	0.035	0.27	0.090
350	0.25	0.040	0.29	0.093
400	0.23	0.032	0.26	0.10
450	0.24	0.035	0.27	0.090
500	0.24	0.038	0.28	0.095
550	0.22	0.050	0.27	0.097
600	0.19	0.054	0.25	0.099

C. Appearance potentials

The appearance potentials of the ionic products and the ion pairs are shown in Table V. The existing experimental results are also included. The data in the row of *limit* are the thermochemical limits of the different dissociation channels. Those in the row of *calculated* are calculated assuming that the potential curves of the corresponding ion pair are Coulomb-like and the internuclear distance is at the outer tuning point of the Franck-Condon region. From Table V we see that the appearance potential of $C^{+}+O^{+}$ is considerably below the calculated results. However, for the ion-pair channels after the triple and quadruple ionization, the appearance potentials are in fairly good agreement with the calculated results.

IV. DISCUSSION

When we plot the total cross sections of the different ionization stages at 600 eV versus the ionization stage, we observed a surprising result. As illustrated in Fig. 9, the total cross section shows a very good exponential decrease as the ionization stage increases. The cross section can be described by

$$\sigma(q)=\sigma(1)\exp[-(q-1)/T], \tag{20}$$

where q is the stage of ionization. $\sigma(1)$ is the cross section for single ionization. The numerical fit gives a value of 0.3489 for T. The quantum-mechanical principle shows that the ionization cross section is proportional to the state density, the transition probability from the ground state of neutral molecules, and the inverse of the electron velocity [27].

TABLE V. Appearance potentials (in eV) of the fragments and the ion pairs in the multiple ionization of CO.

Reference	C^{2+}	O^{2+}	CO^{2+}	C^{3+}	$C^{+}+O^{+}$	$C^{2+}+O^{+}$	$C^{+}+O^{2+}$	$C^{2+}+O^{2+}$	$C^{3+}+O^{+}$
Present work	60.0±3	70.0±3	41.0±2	100±5	37.0±2	84±3	93±3	150±5	150±5
[39]	54.2±0.2	61.8±0.3							
[10]			40.75±0.5		38.4±0.5	81±2			
[40]			41.25±0.05						
[22]						84±3	95±4		
[11]	56.4±1	70±1	41.3±0.2		38.4	82±2			
limit	45.75	59.87		93.6	35.98	59.36	71.13	94.51	107.22
calculated					48.2	83.8	95.6	143.4	143.9

In electron-impact excitation, the electrons can activate all the possible transitions with energies smaller than the electron energy. The ionization cross sections give us the information of the integral of the state density and the transition probability from neutral to multiply ionized molecules. The relation observed in the present experiment shows that this integral decreases exponentially as the ionization stage increases. In the very recent work on N_2 and O_2 of the present authors, similar relations were also observed [37].

Previous experiments on the multiple ionization of molecules have been focused on high-intensity laser field ionization [38] and heavy-particle collisions [18]. The authors measured the kinetic-energy release in the fragmentation and interpreted the kinetic-energy distribution of the fragments by Coulomb-like or non-Coulomb-like models. In a very recent theoretical work [23] Handke *et al.* pointed out that the multiple ionization of molecules is related to numerous electronic states up to very high energies; the overall kinetic-energy distribution of the fragments cannot be explained by the models that just consider the lowest electronic levels. Here we multiplied the total cross section σ_t by $\sqrt{E}$. We thus got approximate values for the integrals of the products of the electronic state density and the transition probability over electron energy for singly, doubly, triply, and quadruply ionized CO, respectively [27]. The results are shown in Fig. 10. We see that the $\sigma_t\sqrt{E}$ values increase with increasing electron energy and reach a constant value at approximately the electron energies of 80, 180, 230, and 500 eV for single, double, triple, and quadruple ionization, respectively. This suggests that at high excitation energies, the electronic states at energies as high as 80, 180, 230, and 500 eV may contribute to the single, double, triple, and quadruple ionization, respectively. The result therefore supports the conclusion of Handke *et al.* [23]. In the work of high-intensity laser field ionization [38] and heavy-particle collisions [18], where the excitation energy is comparable to or even exceeds that in electron-impact ionization, the contribution to the fragmentation of the multiply ionized molecules can originate from very high electronic states. It is thus not reasonable to conclude whether the dissociation is via Coulomb-like or non-Coulomb-like potential energy curves by just considering only the lowest electronic states. The kinetic-energy release may have complex distributions since numerous and very high electronic states are involved.

The three-hole population analysis of Handke *et al.* [23] (Fig. 2 in [23]) shows that after the triple ionization of CO, the $C^{-1}O^{-2}$ character (one hole on C and the other two on O) has an importance similar to $C^{-2}O^{-1}$. If we check their calculation further we see that the CO^{-3} character also has an overall importance similar to $C^{-3}O$ at higher excitation energies. However, the present cross-section measurements show that not only does the channel $C^{2+}+O^{+}$ have a much higher cross section than $C^{2+}+O^{+}$, but $C^{3+}+O$ has a much higher cross section than $C+O^{3+}$. This result supports another conclusion of Handke *et al.* [23], namely, that the dissociation of the multiply ionized molecules does not proceed along potential curves. During the dissociation the nuclei may gain considerable momentum and jump from one curve

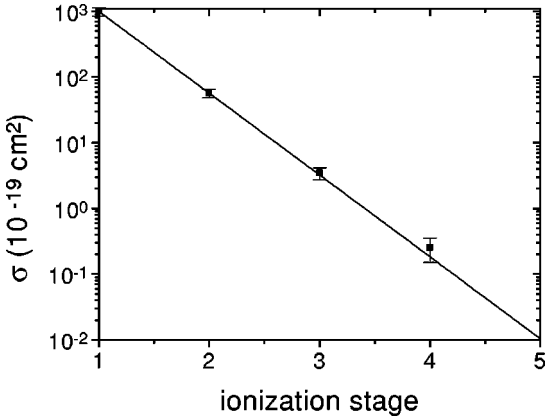

FIG. 9. Total cross sections of different stages of ionization at 600 eV versus the ionization stage. The experimental results are fitted to an exponential decay.

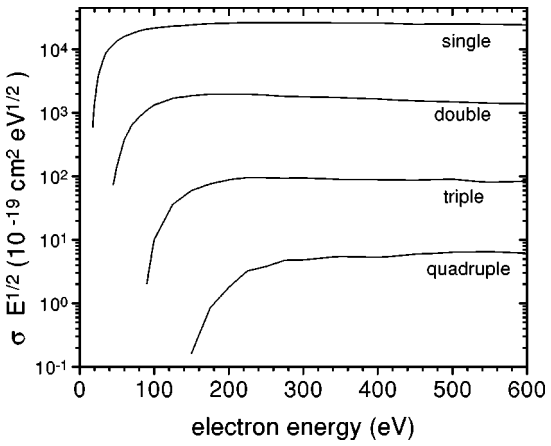

FIG. 10. Dependence of $\sigma\sqrt{E}$ on electron energy for single, double, triple, and quadruple ionization.

to another. Experiment shows that the preference of the channels is always related to their dissociation limits. The channel with a lower dissociation limit has a higher preference in dissociation. This is the case not only for triply ionized CO, but also for singly, doubly, and quadruply ionized CO.

The appearance potential measurements reveal some information about the lowest potential curves of the molecules at different ionization stages. For double ionization from Table V we see that the appearance potentials for CO^{2+} and $C^+ + O^+$ are considerably lower than that predicted by the pure Coulomb-like curve. This is because the bond interaction of C^+ and O^+ generates some metastable states with shallow potential wells in the Franck-Condon region [16]. We see that the appearance potential of CO^{2+} is in good agreement with the calculation. The appearance potential of $C^+ + O^+$ is lower than that of CO^{2+}; this is due to the contribution of the autoionization of $CO^{+}*$.

For triple ionization, the appearance potential of the ion pair $C^{2+} + O^+$ is in good agreement with the prediction of a pure Coulomb-like potential curve. This suggests that the lowest electronic state of CO^{3+} is nearly Coulomb-like. Almost no shallow potential well can exist on this curve because the Coulomb-like interaction of the C^{2+} and O^+ are stronger. The appearance potential of $C^+ + O^{2+}$ is close to what is predicted by a Coulomb-like curve, although complex dissociation dynamics are involved. In the case of quadruple ionization, where the Coulomb-like interaction is even stronger, the appearance potentials of the ion pairs of $C^{2+} + O^{2+}$ and $C^{3+} + O^+$ are close to those predicted by the Coulomb-like potential curves.

V. CONCLUSIONS

We report the measurements of the absolute cross sections of all the possible dissociation channels following the electron-impact multiple ionization of CO. The electronic states of the multiply ionized molecules are usually located well above the dissociation limits because of the Coulomb-like interaction of the charged pairs. The fragments from the dissociation of the multiply ionized molecules carry the kinetic energies as high as tens of eV, which makes it very difficult to collect the fast ions. In order to measure the dissociation channels of the multiply ionized molecules, the ionic fragments have to be measured exclusively and selectively and coincidence techniques have to be used. The present experiment was done in the focusing time-of-flight mass spectrometer developed by the present authors, which has high capability in collecting fast ions. Two coincidence techniques have been developed to measure the absolute cross sections of ion-pair productions. The cross sections of the channels corresponding to the production of ion pairs are measured by the coincidence techniques. Those of the channels associated with neutral fragments are obtained indirectly. Generally, the error in the measurement is about 15% if the cross section value is not extremely small. At high excitation energies the total cross sections of different stages of ionization show an exponential decrease as the ionization stage increases. The cross sections of the different channels reveal the internal dissociation dynamics of dissociation following the multiple ionization of molecules and support the very recent theoretical work of Handke *et al.* [23]. The appearance potentials corresponding to different dissociation channels are also measured, which show that the ground states of triply and quadruply ionized CO are nearly Coulomb-like because the Coulomb-like interactions inside the molecules are stronger.

ACKNOWLEDGMENTS

One of the authors (C. T.) is grateful to the Alexander von Humboldt Foundation for financial support for staying at the Max-Planck-Institute for Extraterrestrial Physics. The technical support of B. Steffes and the stimulating discussions with T. Sykora are also appreciated.

[1] M. Larsson, Comments At. Mol. Phys. **29**, 39 (1993), and references therein.
[2] P. C. Cosby, R. Möller, and H. Helm, Phys. Rev. A **28**, 766 (1987).
[3] A. S. Mullin, D. M. Szaflarski, K. Yokoyama, G. Gerber, and W. C. Lineberger, J. Chem. Phys. **96**, 3636 (1992).
[4] M. Larsson and G. Sunström, J. Chem. Phys. **97**, 1750 (1992).
[5] D. Cossart and M. Bonneau, J. Mol. Spectrosc. **125**, 413 (1987).
[6] D. Cossart and C. Cossart-Magos, J. Mol. Spectrosc. **147**, 471 (1991).
[7] M. Hochlaf, R. I. Hall, F. Penent, H. Kjedsen, P. Lablanquie, M. Lavollee, and J. H. D. Eland, Chem. Phys. **207**, 159 (1996).
[8] G. Dawber, A. G. McConkey, L. Avald, M. A. MacDonald, G. C. King, and R. I. Hall, J. Phys. B **27**, 2191 (1994).
[9] M. J. Besnard, L. Hellner, G. Dujardin, and D. Winkoun, J. Chem. Phys. **88**, 1732 (1988).
[10] P. Lablanquie, J. Delwiche, M.-J. Hubin-Franskin, I. Nenner, P. Morin, K. Ito, J. H. D. Eland, J.-M. Robbe, G. Gandara, J. Fournier, and P. G. Fournier, Phys. Rev. A **40**, 5673 (1989).
[11] T. Masuoka and E. Nakamura, Phys. Rev. A **48**, 4379 (1993).
[12] T. Masuoka, J. Chem. Phys. **101**, 322 (1994).
[13] T. Masuoka, E. Nakamura, and A. Hiraya, J. Chem. Phys. **104**, 6200 (1996).
[14] M. R. Bruce, L. Mi, C. R. Sporleder, and R. A. Bonham, J. Phys. B **27**, 5773 (1994).
[15] E. Faonelli, F. Maracci, and R. Platania, J. Chem. Phys. **101**, 6565 (1994).
[16] R. W. Wetmore and R. K. Boyd, J. Phys. Chem. **90**, 5540 (1986).
[17] P. R. Talor and H. Partridge, J. Phys. Chem. **91**, 6148 (1987).
[18] G. Sampoll, R. L. Watson, O. Heber, V. Horvat, K. Wohrer, and M. Chabot, Phys. Rev. A **45**, 2903 (1992).
[19] D. Mathur, E. Krishnakumar, K. Nagesha, V. R. Marathe, V. Krishmurth, F. A. Rajgara, and U. T. Raheja, J. Phys. B **26**, L141 (1993).
[20] L. J. Frasinski, K. Codling, and P. A. Hatherly, Science **246**, 1029 (1989).

[21] L. J. Frasinski, P. A. Hatherly, K. Codling, M. Larson, A. Persson, and C.-G. Wahlström, J. Phys. B **27**, L109 (1994).
[22] G. Spekowius, and B. Brehm, Chem. Phys. Lett. **187**, 442 (1991).
[23] G. Handke, F. Tarantelli, and L. S. Cederbaum, Phys. Rev. Lett. **76**, 896 (1996).
[24] G. Handke, F. Tarantelli, and A. Sgamellotti, J. Chem. Phys. **104**, 9531 (1996).
[25] G. Handke, F. Tarantelli, A. Sgamellotti, and L. S. Cederbaum, J. Electron Spectrosc. Relat. Phenom. **76**, 307 (1995).
[26] Cechan Tian and C. R. Vidal, J. Phys. B **31**, 895 (1998).
[27] A. Messiah, *Quantum Mechanics* (North-Holland, Amsterdam, 1961), Vol. 2.
[28] Cechan Tian and C. R. Vidal, J. Chem. Phys. **108**, 927 (1998).
[29] Cechan Tian and C. R. Vidal, Phys. Rev. A **58**, 3783 (1998).
[30] C. Ma, M. R. Bruce, and R. A. Bonham, Phys. Rev. A **44**, 2921 (1991).
[31] B. Brehm, J. Grosser, T. Ruscheinski, and M. Zimmer, Meas. Sci. Technol. **6**, 953 (1995).
[32] H. C. Straub, P. Renault, B. G. Lindsay, K. A. Smith, and R. F. Stebbings, Phys. Rev. A **52**, 1115 (1995).
[33] R. Locht, Chem. Phys. **22**, 13 (1977).
[34] T. Nakano, H. Toyoda, and H. Sugai, Jpn. J. Appl. Phys., Part 1 **30**, 2908 (1991); **30**, 2912 (1991); H. Toyoda, M. Iio, and H. Sugai, *ibid.* **36**, 3730 (1997).
[35] P. J. M. Van der Burgt and J. W. McConkey, J. Phys. B **24**, 4821 (1991); L. R. Leclair, J. M. Derbyshire, and J. W. McConkey, J. Geophys. Res. **101**, E7585 (1996); L. R. LeClair, M. D. Brown, and J. W. McConkey, Chem. Phys. **189**, 769 (1994).
[36] P. C. Cosby, J. Chem. Phys. **98**, 7804 (1993).
[37] Cechan Tian and C. R. Vidal, J. Phys. B **31**, 5369 (1998).
[38] See, for example, W. T. Hill III, J. Zhu, D. L. Hatten, Y. Cui, J. Goldhar, and S. Yang, Phys. Rev. Lett. **69**, 2646 (1992).
[39] P. M. Hierl and J. L. Franklin, J. Chem. Phys. **47**, 3154 (1967).
[40] G. Dujardin, L. Hellner, M. Hamdan, A. G. Brenton, B. J. Olsson, and M. J. Besnard-Ramage, J. Phys. B **23**, 1165 (1990).